Supplementary Information

Metal nanoparticles at grain boundaries of titanate toward efficient carbon dioxide electrolysis

Zhibo Shang,[abcd] Jie Zhang,[abcd] Lingting Ye *[bcd] and Kui Xie*[abcd]

[a]*College of Chemistry, Fuzhou University, Fuzhou 350108, Fujian, China. E-mail: kxie@fjirsm.ac.cn; Fax: +86-591-63179173; Tel: +86-591-63179173*

[b]*Fujian Science & Technology Innovation Laboratory for Optoelectronic Information of China, Fuzhou, Fujian 350108, China. E-mail: ltye@fjirsm.ac.cn*

[c]*Key Laboratory of Optoelectronic Materials Chemistry and Physics, Fujian Institute of Research on the Structure of Matter, Chinese Academy of Sciences, Fuzhou, Fujian 350002, China.*

[d]*Key Laboratory of Design & Assembly of Functional Nanostructures, Chinese Academy of Sciences, Fuzhou, Fujian 350002, China.*

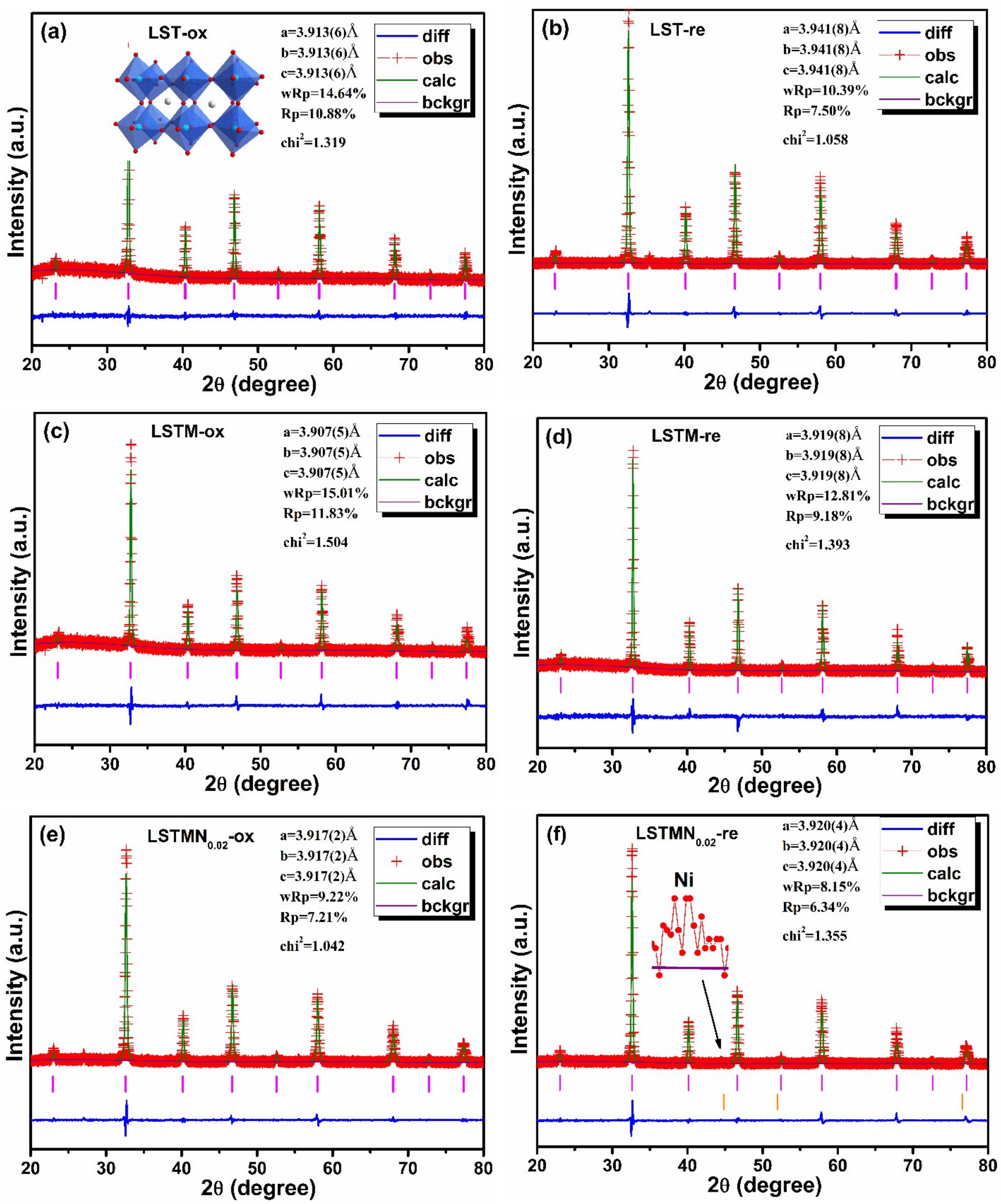

Fig. S1 XRD rietveld refinement patterns of the (a) oxidized and (b) reduced LST; (c) oxidized and (d) reduced LSTM; (e) oxidized and (f) reduced $LSTMN_{0.02}$.

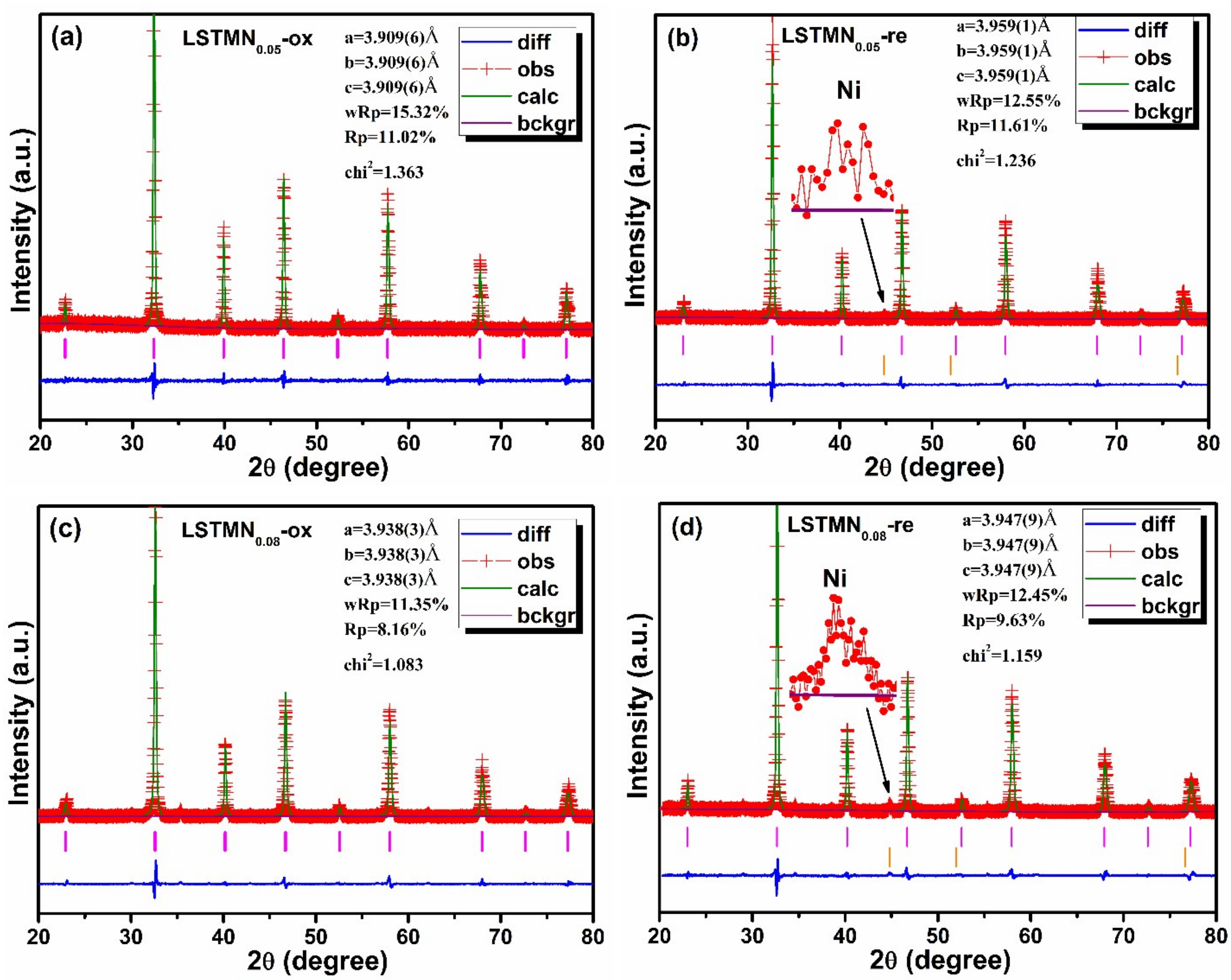

Fig. S2 XRD rietveld refinement patterns of the (a) oxidized and (b) reduced $LSTMN_{0.05}$; (c) oxidized and (d) reduced $LSTMMN_{0.08}$.

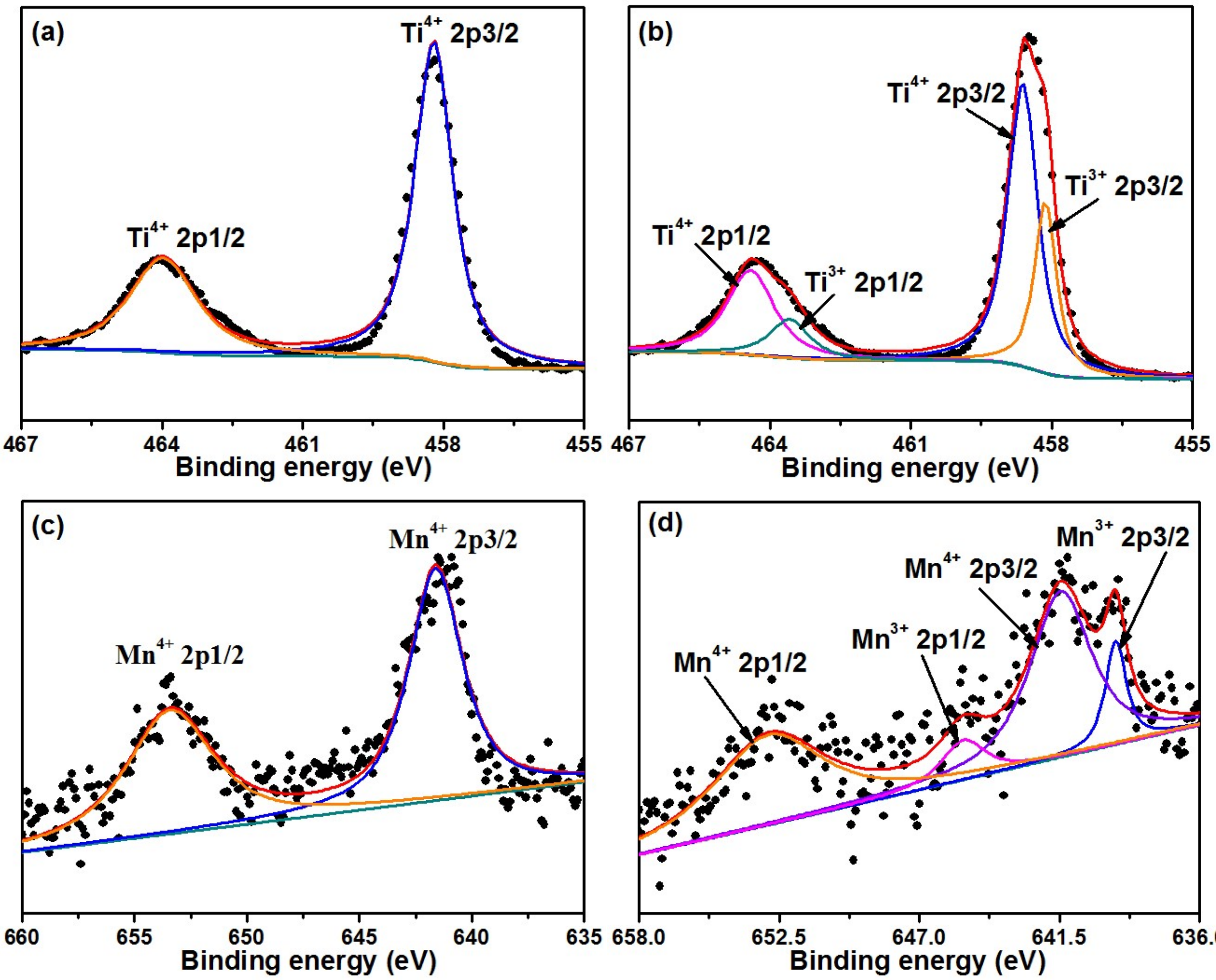

Fig. S3 XPS results of Ti and Mn in the (a, c) oxidized and (b, d) reduced LSTM, respectively.

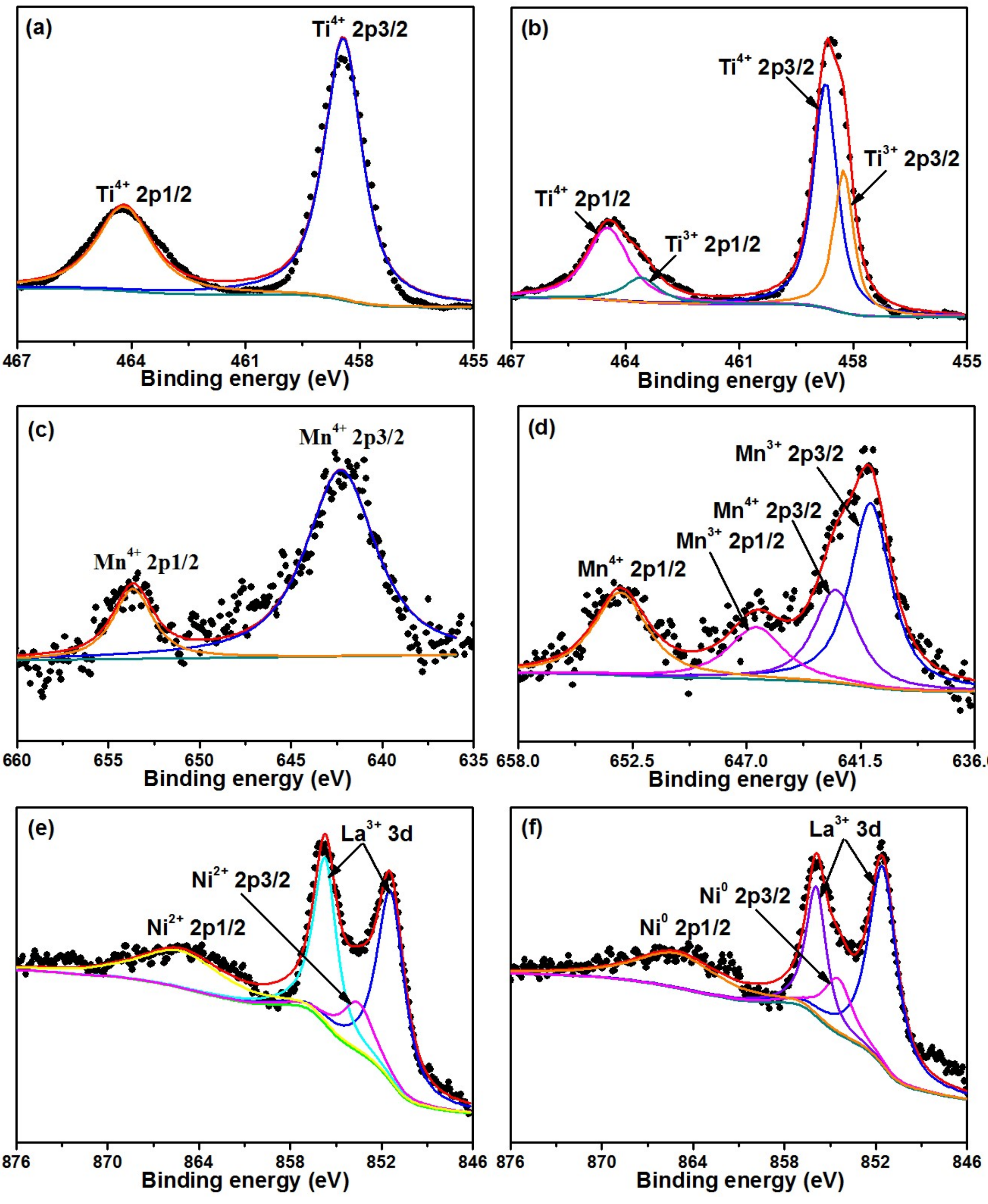

Fig. S4 XPS results of Ti, Mn and Ni in the (a, c, e) oxidized and (b, d, f) reduced $LSTMN_{0.1}$, respectively.

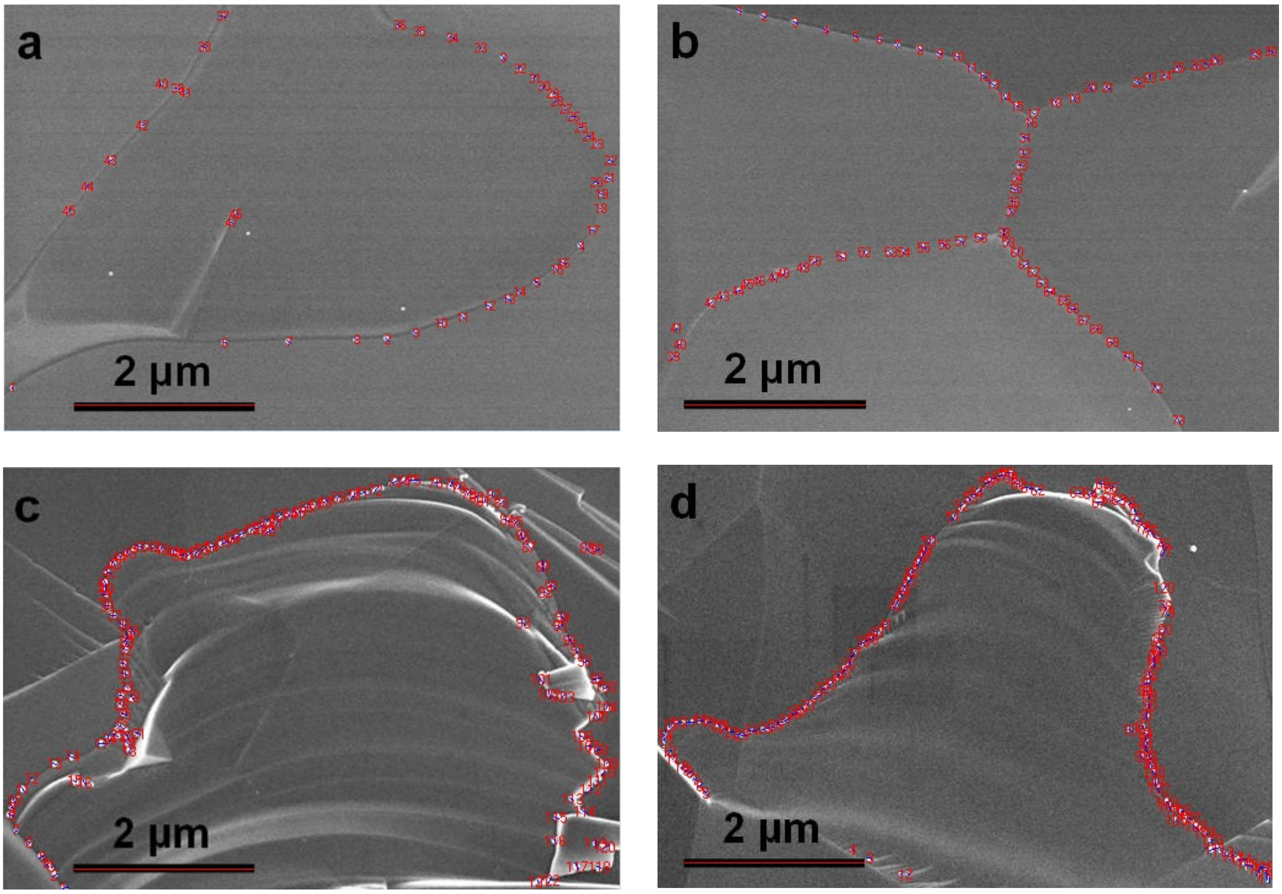

Fig. S5 The number of all selected nickel nanoparticles at grain boundaries in titanate from the SEM results for the reduced (a) $LSTMN_{0.02}$, (b) $LSTMN_{0.05}$, (c) $LSTMN_{0.08}$ and (d) $LSTMN_{0.1}$.

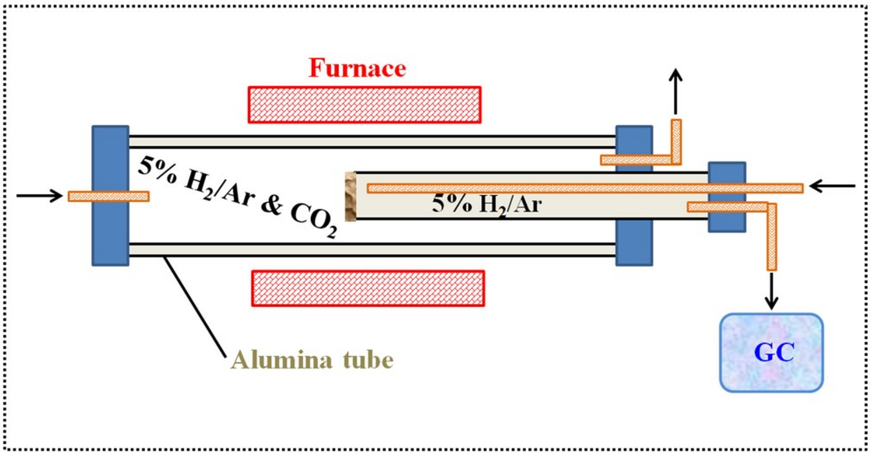

Fig. S6 Schematic illustration of oxygen permeation flux measurement device.

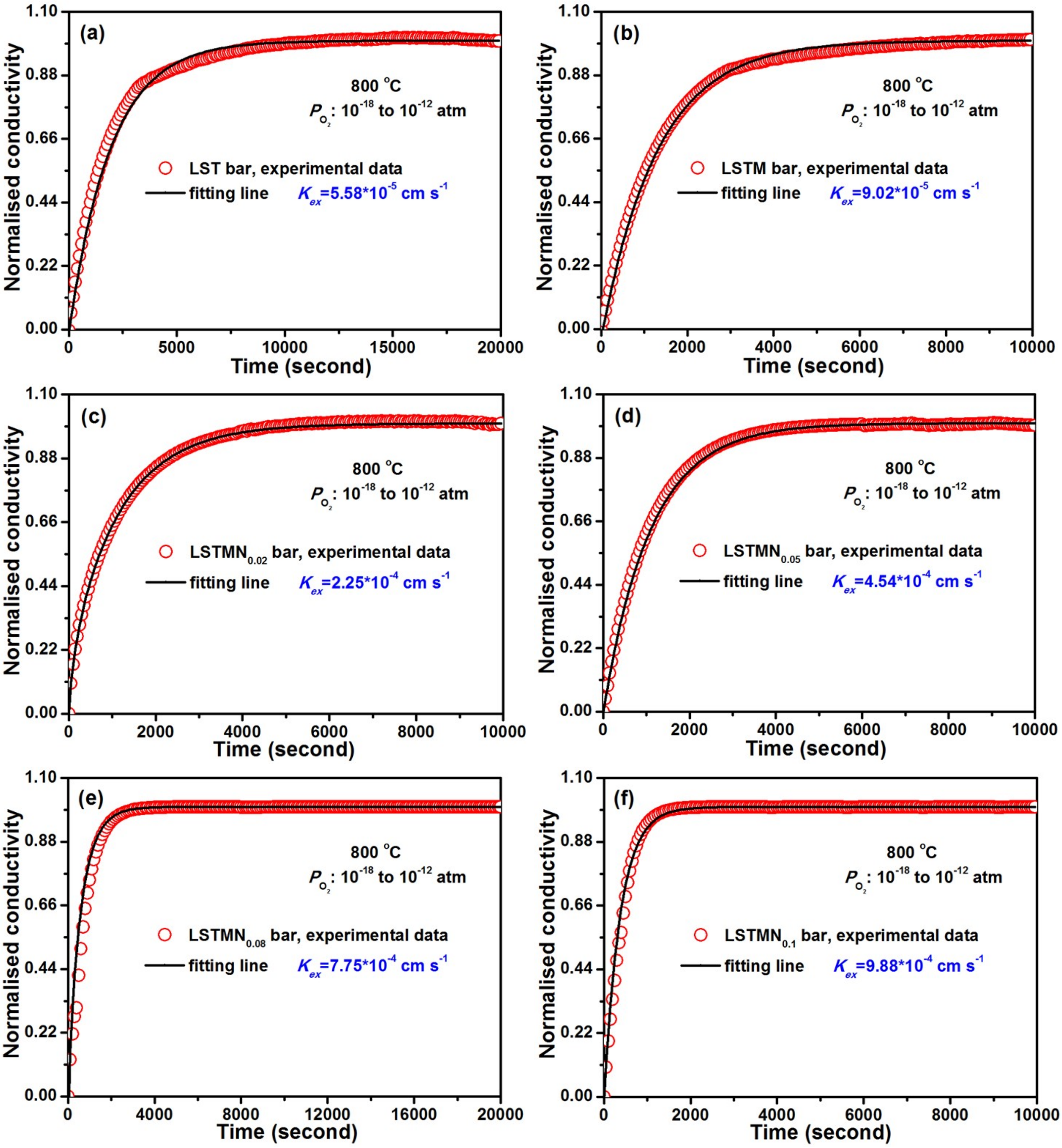

Fig. S7 Electrical conductivity relaxation curves of reduced (a) LST, (b) LSTM, (c) $LSTMN_{0.02}$, (d) $LSTMN_{0.05}$, (e) $LSTMN_{0.08}$ and (f) $LSTMN_{0.1}$ at 800 °C.

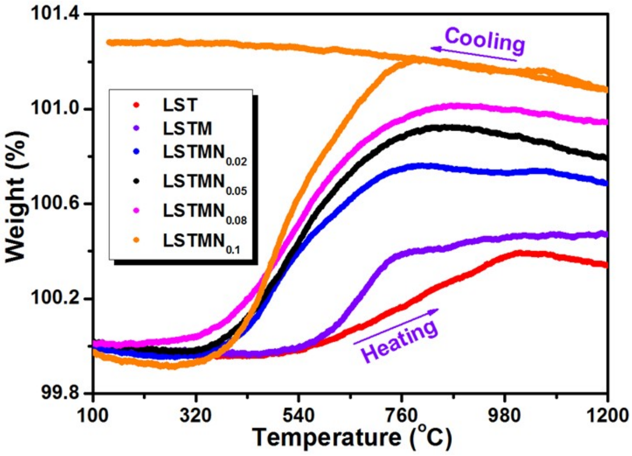

Fig. S8 TGA tests of the reduced samples from 100 to 1200 °C in air.

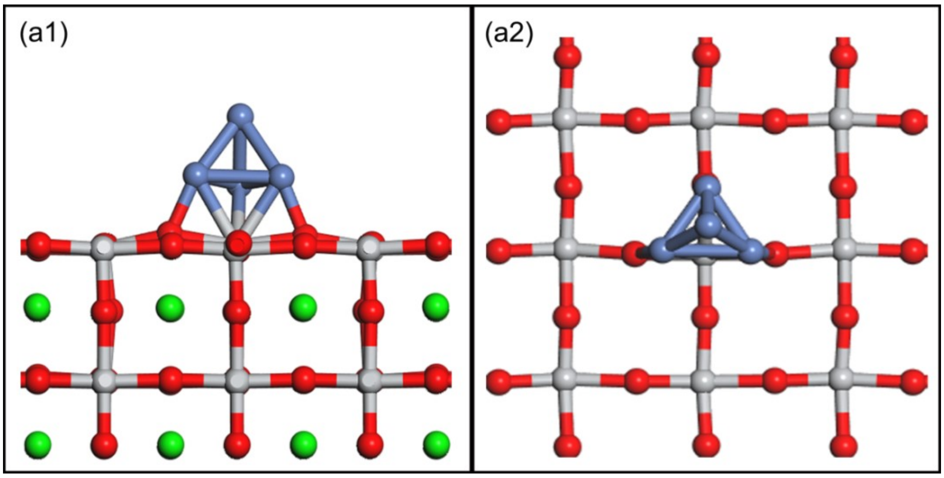

Fig. S9 The configurations of clean (001) Ni/STO system surface, and the left panel shows side view while right panel gives top view. Nickel in blue, strontium in green, titanium in pale and oxygen in red.

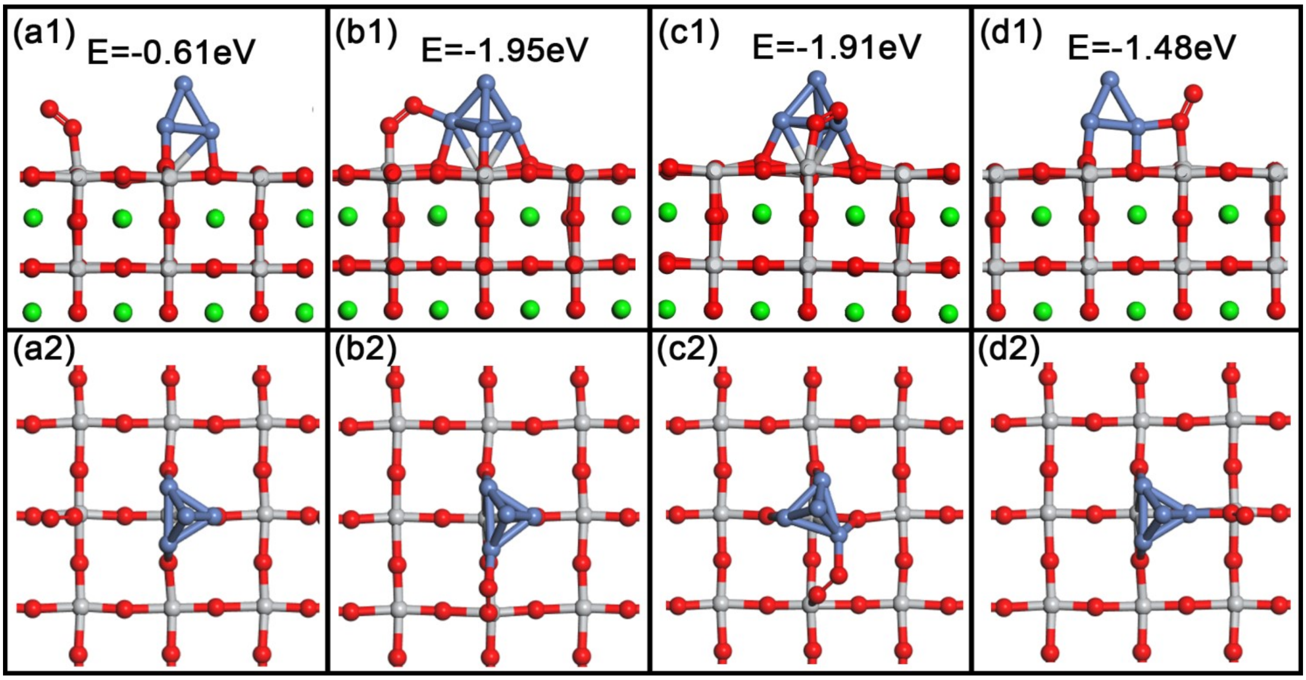

Fig. S10 Different adsorption configurations of O_2 on the (001) Ni/STO system surface. And each O_2 chemisorption energy is given on the top of configuration with eV unit. Nickel in blue, strontium in green, titanium in pale and oxygen in red.

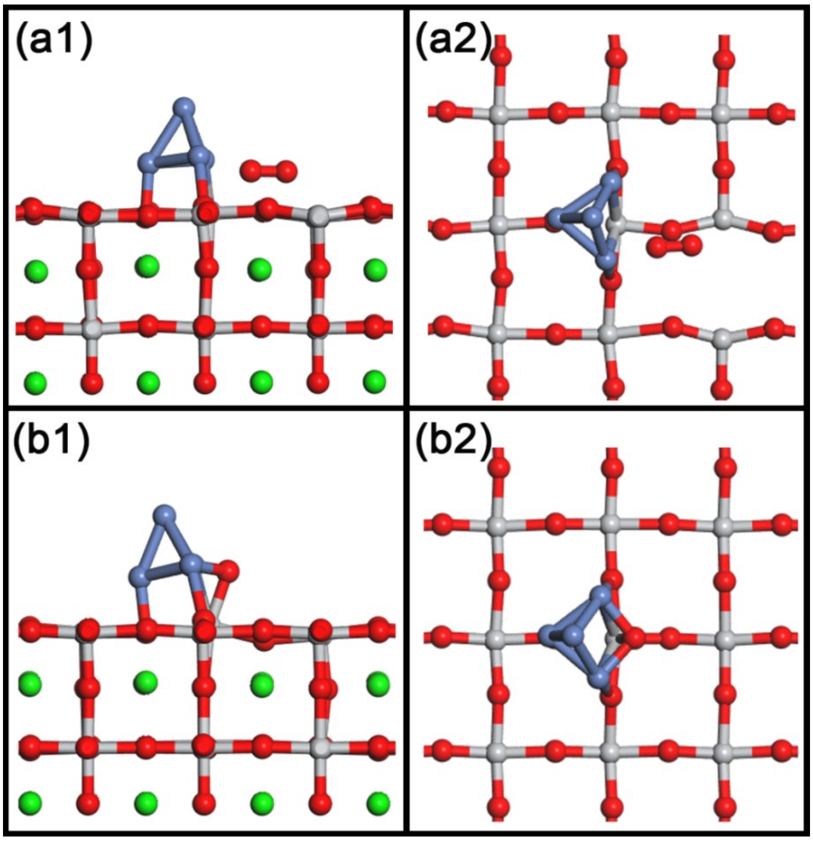

Fig. S11 (a) The original configurations of O_2 approach to defected site of the (001) Ni/STO surface system; (b) the optimization configurations of O_2 approach to defected site of the (001) Ni/STO surface system. Left panels show side views while right panels give top views. Nickel in blue, strontium in green, titanium in pale and oxygen in red.

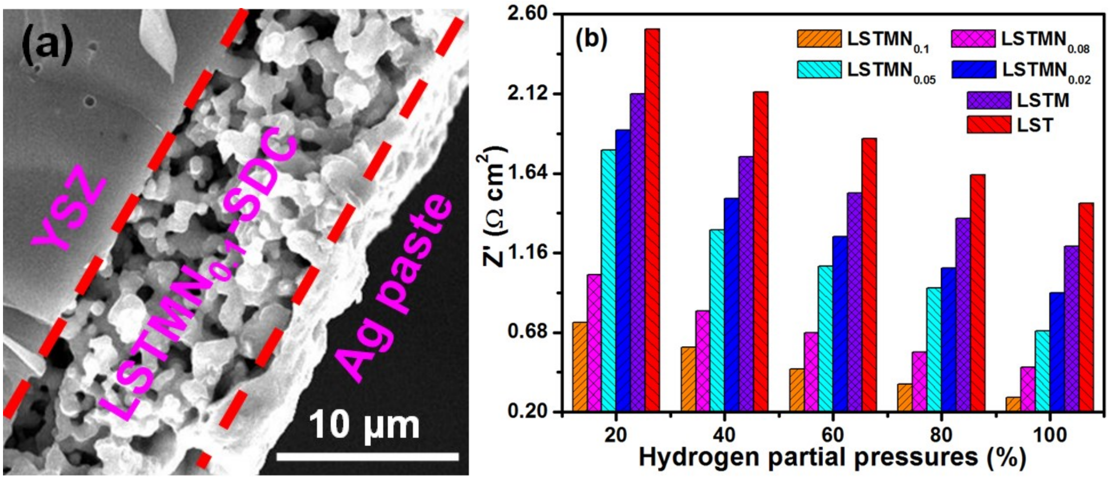

Fig. S12 (a) SEM picture of the $LSTMN_{0.1}$-SDC electrode on the YSZ electrolyte; (b) the AC impendence of the symmetric cells for samples at various H_2 partial pressures at 800 ^{o}C.

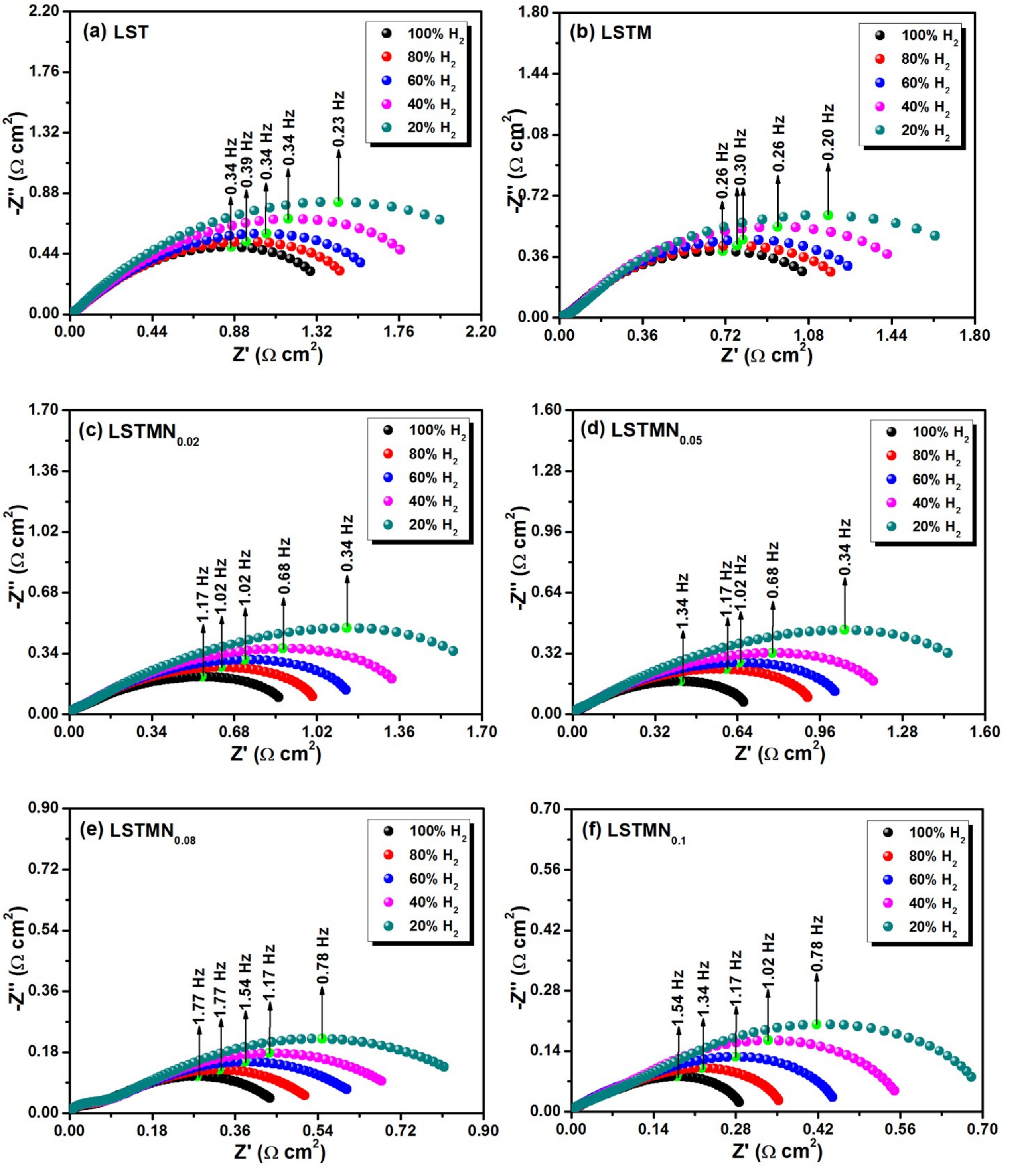

Fig. S13 The AC impendence of the symmetric cells for (a) LST, (b) LSTM, (c) $LSTMN_{0.02}$, (d) $LSTMN_{0.05}$, (e) $LSTMN_{0.08}$ and (f) $LSTMN_{0.1}$ at various H_2 partial pressures at 800 ^{o}C.

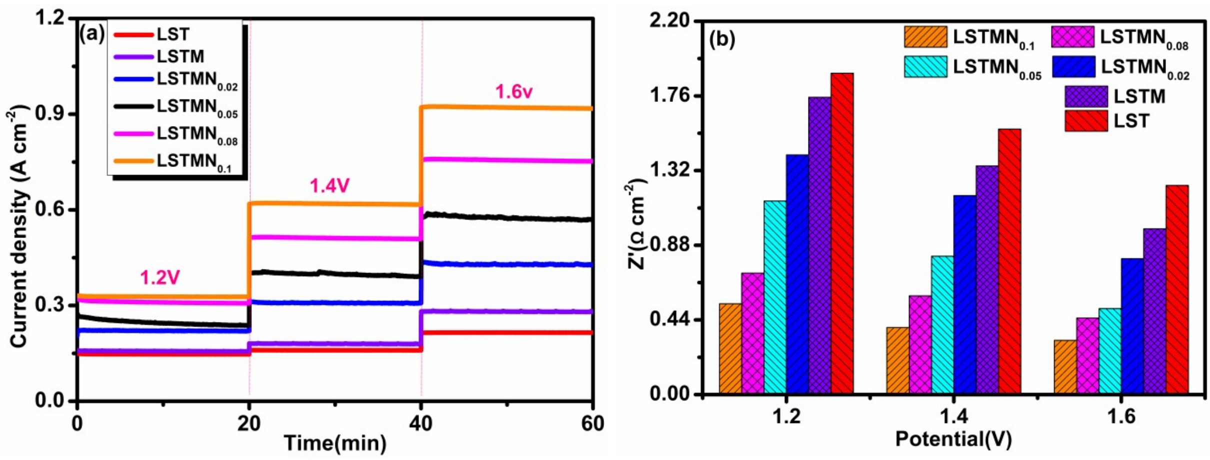

Fig. S14 (a) The short-term performances of CO_2 electrolysis at different voltages; (b) Comparison of R_p for high-temperature CO_2 electrolysis with different electrodes.

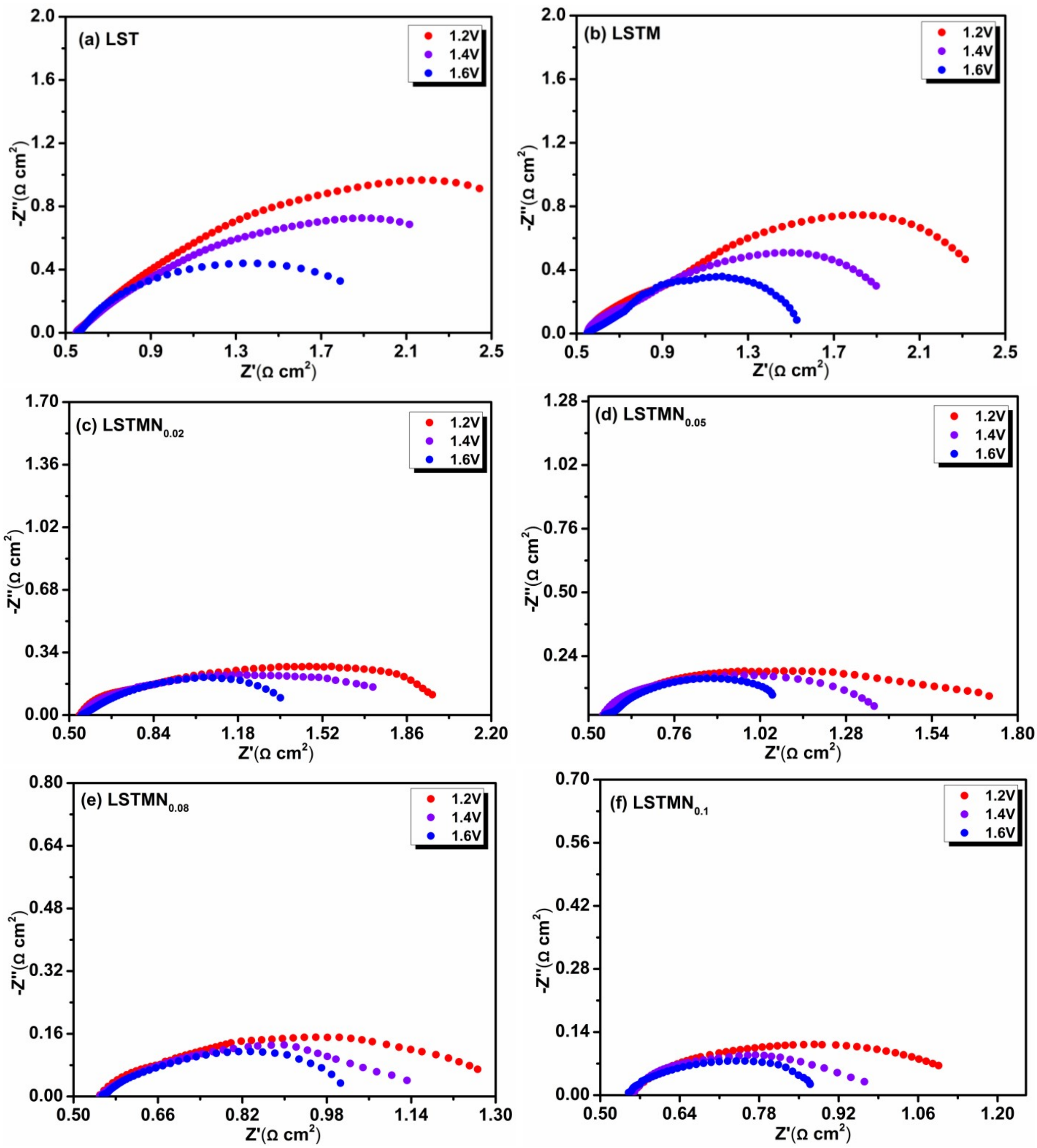

Fig. S15 *In situ* AC impendence for electrolysers based on (a) LST, (b) LSTM, (c) $LSTMN_{0.02}$, (d) $LSTMN_{0.05}$, (e) $LSTMN_{0.08}$ and (f) $LSTMN_{0.1}$ at various voltages.

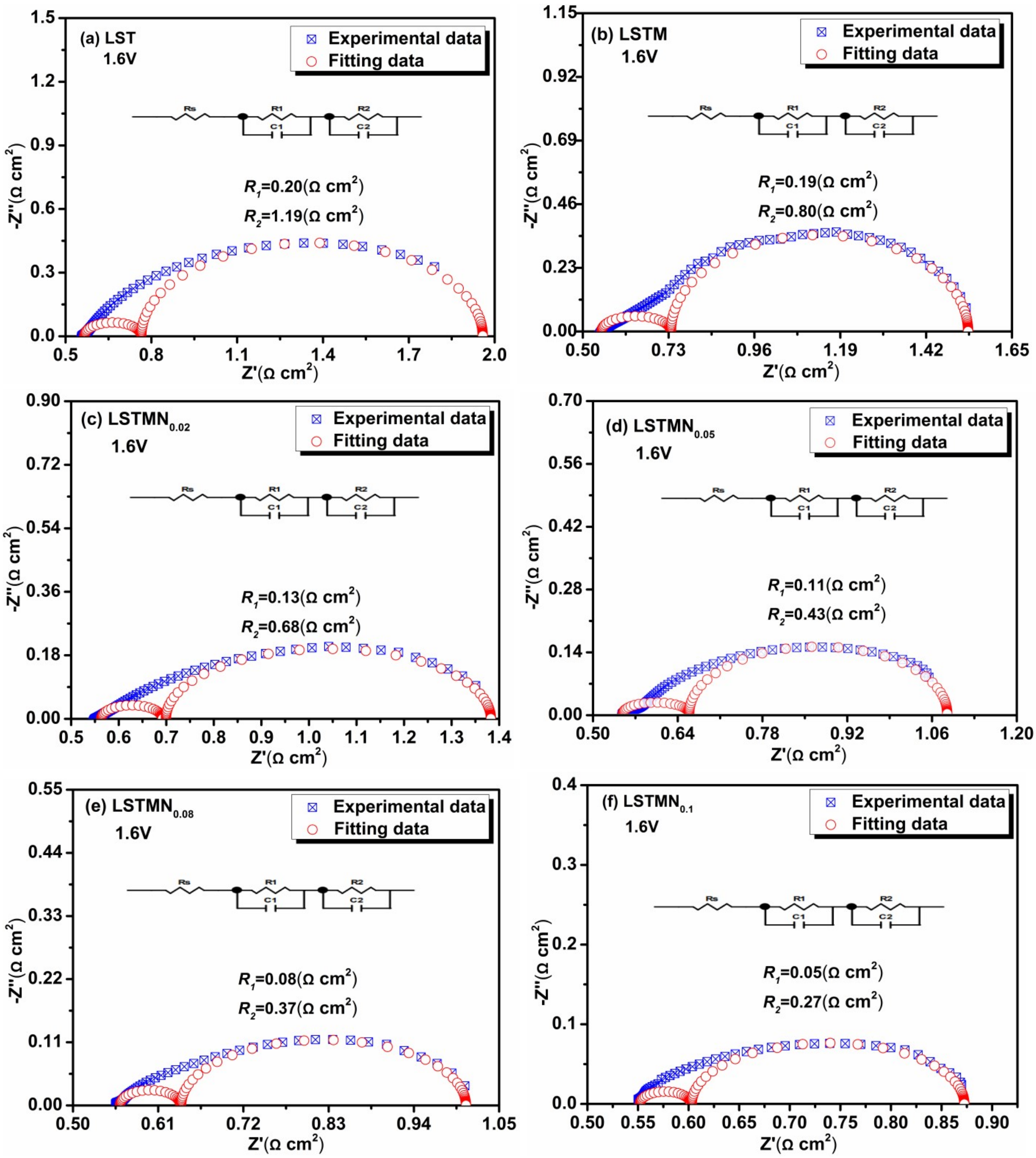

Fig. S16 *In situ* AC impendence for electrolysers based on (a) LST, (b) LSTM, (c) $LSTMN_{0.02}$, (d) $LSTMN_{0.05}$, (e) $LSTMN_{0.08}$ and (f) $LSTMN_{0.1}$ at 1.6 V by Zview fitting.

Table S1 The P''_{O_2} and P'_{O_2} represent the oxygen partial pressure on the feed and permeated side, respectively.

	600 °C	650 °C	700 °C	750 °C	800 °C
P''_{O_2} (Pa)	1.268×10^{-19}	3.004×10^{-19}	8.305×10^{-19}	5.606×10^{-18}	6.885×10^{-17}
P'_{O_2} (Pa)	1.641×10^{-21}	3.809×10^{-21}	9.826×10^{-21}	6.069×10^{-20}	7.005×10^{-19}
P''_{O_2}/ P'_{O_2}	77.27	78.87	84.52	92.37	98.29
$\ln(P''_{O_2}/ P'_{O_2})$	4.347	4.368	4.437	4.526	4.588